Remote Sensing of Environment 115 (2011) 1003–1012

Contents lists available at ScienceDirect

Remote Sensing of Environment

journal homepage: www.elsevier.com/locate/rse

Mapping burned areas from Landsat TM/ETM+ data with a two-phase algorithm: Balancing omission and commission errors

Aitor Bastarrika [a], Emilio Chuvieco [b,*], M. Pilar Martín [c]

[a] Department of Surveying Engineering, University of the Basque Country, Spain
[b] Department of Geography, University of Alcalá, Spain
[c] Center of Human and Social Sciences, National Research Council (CSIC), Spain

ARTICLE INFO

Article history:
Received 1 May 2010
Received in revised form 3 November 2010
Accepted 4 December 2010
Available online 15 January 2011

Keywords:
Burned areas
Contextual algorithms
Landsat TM/ETM+ images
Logistic regression

ABSTRACT

Maps of burned area have been obtained from an automatic algorithm applied to a multitemporal series of Landsat TM/ETM+ images in two Mediterranean sites. The proposed algorithm is based on two phases: the first one intends to detect the more severely burned areas and minimize commission errors. The second phase improves burned patches delimitation using a hybrid contextual algorithm based on logistic regression analysis, and tries to minimize omission errors. The algorithm was calibrated using six study sites and it was validated for the whole territory of Portugal (89,000 km^2) and for Southern California (70,000 km^2). In the validation exercise, 65 TM/ETM+ scenes for Portugal and 35 for California were used, all from the 2003 fire season. A good agreement with the official burned area perimeters was shown, with kappa values close to 0.85 and low omission and commission errors (<16.5%). The proposed algorithm could be operationally used for historical mapping of burned areas from Landsat images, as well as from future medium resolution sensors, providing they acquire images in two bands of the Short Wave Infrared (1.5–2.2 μm).

1. Introduction

Biomass burning is widely recognized as one of the critical factors affecting vegetation succession and carbon budgets worldwide (Chuvieco, 2008; Thonicke et al., 2010). It has many socio-economic implications, especially in developed countries where the growing urbanization of forested areas tends to increase accidents associated with extreme fire events. Australia, Greece, Portugal, Russia or California have been seriously affected by severe fires in the last few years. At a global scale, the effects of fire on the atmospheric chemistry are one of the most complex factors to account for in the current emission models (Randerson et al., 2005). The estimations are typically based on the amount of biomass consumed, and this requires accurate mapping of burned areas, as well as knowing the combustion completeness of fires and having pre-fire biomass assessments (Palacios-Orueta et al., 2005).

Mapping of burned areas at global scale using satellite images has been mostly based on coarse spatial resolution data such as Advanced Very High Resolution Sensor (AVHRR), VEGETATION or Moderate Resolution Imaging Spectroradiometer (MODIS) images. However, the requisites of the climate modelling community are not yet met with the current satellites (GCOS, 2006), as these sensors do not provide enough spatial detail. The use of mid-resolution sensors has commonly been oriented toward local-scale studies, but in the last years they have also been used in global studies, both because of the more strict requirements set by the Kyoto protocol (Rosenqvist et al., 2003), and by the growing availability of those images, specially after the Landsat historical archive was placed in the public domain. Landsat Thematic Mapper (TM) and Enhanced Thematic Mapper (ETM+) images have been widely used for mapping burned areas, mostly in local and regional studies (Chuvieco et al., 2002; Hudak & Brockett, 2004; Koutsias & Karteris, 1998; Mitri & Gitas, 2004; Russel-Smith et al., 1997, 2002; Smith et al., 2007). The accuracy of those studies was generally high, but most of them were focused on single sites and did not provide estimations on the potential performance of the proposed algorithms to other sites with different input conditions. Therefore, there is not yet an operationally accepted method to map burned areas from TM-ETM+ images, which could be applicable to a wide variety of fire conditions.

Few countries have operational programs to map burned areas systematically. A notable exception is Portugal, which has performed yearly mapping of burned areas since 1990, based on visual analysis of multitemporal Landsat images (http://www.afn.min-agricultura.pt/portal/dudf/cartografia/cartograf-nac-areas-ardidas-1990-2008 last access September, 1st). The database is now being extended to 1975 using classification techniques. Other countries that have recently undertaken this activity are the US program on mapping burn severity, which includes large fires from 1984 to 2008 (http://www.mtbs.gov/index.html, last access September, 1st).

Burned patches are relatively easy to discriminate visually, but they are complex to detect automatically, because of the wide spatial

* Corresponding author. Tel.: +34 918854438.
E-mail address: emilio.chuvieco@uah.es (E. Chuvieco).

0034-4257/$ – see front matter © 2010 Elsevier Inc. All rights reserved.
doi:10.1016/j.rse.2010.12.005

and spectral diversity caused by the severity of the fire, the time elapsed since the fire was extinguished, and the type of vegetation burned (Chuvieco et al., 2006; Pereira & Setzer, 1993; Pereira et al., 1999b). For this reason, most of the available algorithms try to balance between reducing false detections (commission errors) and increasing detection rate (omission errors). When the detection criteria are very strict, false discriminations are reduced, but many burned pixels remain undetected; the opposite is true when the criteria are looser. In most of the published papers the proposed algorithms are adjusted to the local conditions and therefore obtain reasonable results, but it is not clear whether (they) can be extended to other study sites. The global algorithms developed for coarse resolution images (Riaño et al., 2007; Roy et al., 2005; Tansey et al., 2008b) try to provide more robust approaches while considering the wide range of burn conditions; these generally offer very diverse omission and commission errors in different ecosystems (Roy & Boschetti, 2009; Roy et al., 2008; Tansey et al., 2008a).

An alternative to solve the apparent contradiction between omission and commission errors in mapping burned areas is to apply a two-phase approach. In the first phase the goal would be to reduce the commission errors using strict criteria that would detect only the more clearly burned pixels (seed pixels: "core burned"), even at the cost of omitting many burned pixels within each burned patch. The second phase would analyze only the vicinity of the seed pixels, applying looser criteria to accept as burned those neighbour pixels with similar spectral characteristics to the seeds. This phase would enlarge the burned area to match the whole burned patch, and thus should aim to reduce omission errors. The first proposals for a two-phase mapping method were based on TM/ETM+ images (Chuvieco et al., 2002) but these ideas have also now been explored with medium and low resolution data (Chuvieco, Englefield, et al., 2008; Chuvieco, Opazo, et al., 2008; Fraser et al., 2003; Garcia & Chuvieco, 2004; Maggi & Stroppiana, 2002; Martín, 1998).

This paper presents the performance of a two-phase algorithm developed for burned area mapping based on Landsat TM/ETM+ images, which could be applicable at regional and global scales. To test the generalization power of the algorithm, different study sites have been considered, which include diverse fire conditions within mostly Mediterranean ecosystems. The paper first describes the study sites and the pre-processing steps of the Landsat images and then explains the two phases of the proposed algorithm. The first phase is based on spectral/temporal decision rules, and the second one on contextual techniques.

2. Methods

2.1. Study areas and input data

This study is based on two datasets. The input images to train the different phases of the algorithm were six Landsat TM scenes located in the European Mediterranean basin. They cover diverse areas of Greece, France and Spain, and were acquired before and after fires that mostly affected shrubs and evergreen forested areas (Fig. 1 and Table 1). The validation dataset covered the whole of Portugal and Southern California (Fig. 1) and they were acquired during the 2003 devastating fire season. We downloaded all available TM scenes for those regions from the USGS Global Visualization Viewer (http://www.glovis.usgs.gov/, last access September, 1st), providing they had less than 50% of cloud cover and were acquired between May and December, 2003. Two images acquired at the end of the previous fire season (year 2002) were used to ensure cloud free data for

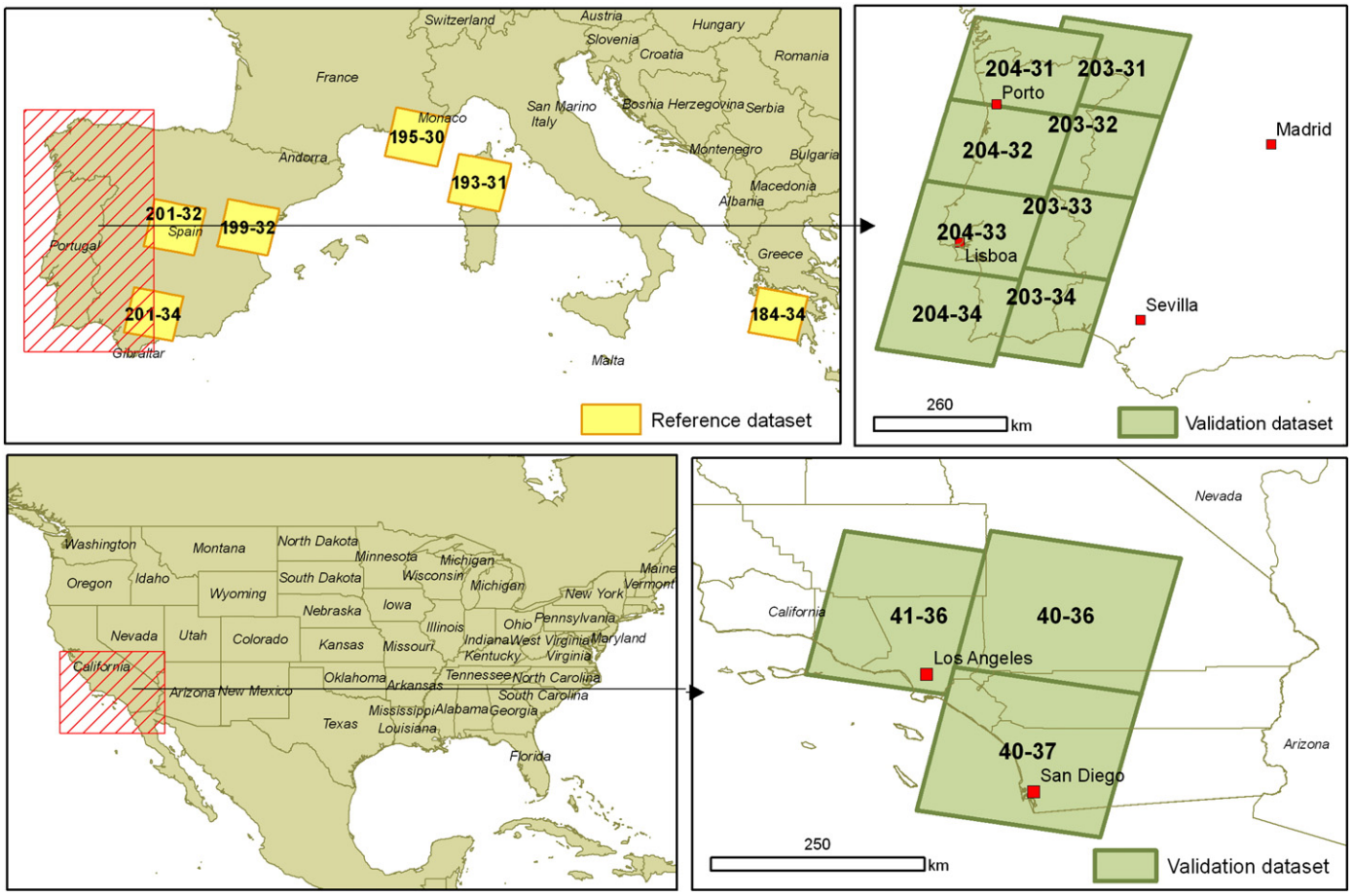

Fig. 1. Location of study sites.

Table 1
Characteristics of the reference study sites.

Name	Localization	Path	Row	Pre-fire image		Post-fire image		Dominant vegetation affected
				Sensor	Date	Sensor	Date	
184-34	Greece	184	34	TM (L5)	29/06/2009	TM (L5)	01/09/2009	Scrub
193-31	Corsica-Sardinia	193	31	TM (L5)	25/06/2002	TM (L5)	16/09/2003	Scrub
195-30	France	195	30	TM (L5)	23/06/2002	TM (L5)	14/09/2003	Scrub and forest
199-32	Spain	199	32	TM (L5)	22/06/2009	TM (L5)	24/07/2009	Forest and scrub
201-32	Spain	201	32	TM (L5)	17/06/2002	TM (L5)	23/08/2003	Scrub and forest
201-34	Spain	201	34	TM (L5)	01/07/2007	TM (L5)	23/08/2009	Scrub

multitemporal comparisons. With those conditions, 65 scenes were processed for Portugal (Table 2) and 35 scenes for Southern California (Table 3).

The Corine Land Cover map of Europe (CLC2000) (http://www.eea.europa.eu/data-and-maps/data/corine-land-cover-2000-clc2000-seamless-vector-database, last access November, 3rd, 2010) and MRLC 2000 Land Cover Database for US (NLCD2000) (Homer et al., 2007) were also available for the study sites. This information was used to detect land cover classes that may offer more confusion with burned areas.

2.2. Validation data

The performance of our algorithm was validated using official fire statistics of the Portuguese and Californian forest services. For Portugal, official fire perimeters are derived from visual analysis of Landsat images. According to these perimeters, 662 fires under 25 ha, 286 fires between 25 and 100 ha, and 238 fires greater than 100 ha (with six large fires higher than 10,000 ha, one of them exceeding 60,000 ha) affected Portugal during the 2003 fire season totalling a burned area of 439,641 ha.

For California, the reference data were based on combined perimeters recorded by several agencies: Bureau of Land Management (BLM), California Department of Forestry and Fire Protection (CDF), National Park Service (NPS) and US Forest Service (USFS) (http://www.frap.cdf.ca.gov/data/frapgisdata/select.asp, last access September, 1st). In Southern California the burned area was estimated in 312,928 ha, with a less burned patches than Portugal: 21 fires under 25 ha, 23 between 25 and 100 ha and 39 greater than 100 ha (with six fires higher than 10,000 ha and one that exceeded 100,000 ha).

Table 2
Landsat TM/ETM+ scenes processed for Portugal.

Path	Row	Year	Day/month (sensor)	No. scenes
204	31	2002	02/09(ETM+), 04/10(ETM+)	2
		2003	25/06(TM), 11/07(TM), 27/07(TM), 12/08(TM), 13/09(TM), 29/09(TM)	6
203	31	2002	25/07(ETM+), 27/09(ETM+)	2
		2003	04/07(TM), 20/07(TM), 05/08(TM), 06/09(TM), 22/09(TM), 08/10(TM)	6
204	32	2002	02/09(ETM+), 04/10(ETM+)	2
		2003	25/06(TM), 11/07(TM), 27/07(TM), 12/08(TM), 13/09(TM), 29/09(TM)	6
203	32	2002	01/07(TM), 29/10(ETM +)	2
		2003	04/07(TM), 20/07(TM), 05/08(TM), 22/09(TM), 08/10(TM)	5
204	33	2002	16/07(ETM+), 02/09(ETM+)	2
		2003	25/06(TM), 11/07(TM), 27/07(TM), 12/08(TM), 13/09(TM),	5
203	33	2002	11/09(ETM+), 29/10(ETM+)	2
		2003	04/07(TM), 20/07(TM), 05/08(TM), 06/09(TM), 22/09(TM), 08/10(TM), 24/10(TM)	7
204	34	2002	16/07(ETM+), 02/09(ETM+)	2
		2003	25/06(TM), 11/07(TM), 27/07(TM), 12/08(TM), 13/09(TM), 29/09(TM), 15/10(TM)	7
203	34	2002	01/07(TM), 29/10(ETM+)	2
		2003	04/07(TM), 20/07(TM), 05/08(TM), 06/09(TM), 22/09(TM), 08/10(TM), 24/10(TM)	7

2.3. Preprocessing of Landsat data

The images downloaded from the Glovis web server included the Standard Terrain Correction (Level 1T), with systematic radiometric and geometric accuracy corrections based on ground control points and a Digital Elevation Model (DEM) for topographic accuracy. Images were converted to Top of the Atmosphere (ToA) reflectance using calibration values included in Chander et al. (2009). Neither atmospheric nor topographic correction was applied.

2.4. Spectral indices for burned land mapping

A literature review was conducted to select the most sensitive input bands to discriminate between burned and unburned pixels. The TM/ETM+ input bands were grouped in three categories according to the different spectral discrimination domains: (a) Visible (VIS, 0.4-0.7 μm) and Near Infrared (NIR, 0.7–1.2 μm); (b) Visible, NIR and 1 band in the Short Wave Infrared (SWIR, 1.5–1.8 μm); (c) Visible, NIR and 2 bands in the SWIR (the second one, between 2 and 2.2 μm). The first spectral domain has been the most commonly used in remote sensing missions, being included in the AVHRR, IRS-WiFS, ENVISAT-MERIS and SPOT-HRV, among others. The second group of bands correspond to more recent environmental sensors, such as the AVHRR-3 (after NOAA-15 at daytime), HRVIR and VEGETATION (both after SPOT-4), LISS and AWIFS (both in Indian IRS satellites). The third group of bands is spectrally the most complete, but it is only covered by a few sensors, such as Landsat TM and ETM+, ASTER and Terra/Aqua-MODIS.

Among the original bands, several spectral indices were included in our analysis in order to enhance the discrimination of burned areas. These indices were used by several authors in burned land mapping studies (Barbosa et al., 1999; Chuvieco et al., 2002; Chuvieco, Englefield, et al., 2008; Fernández et al., 1997; Kasischke & French,

Table 3
Landsat TM/ETM+ scenes processed for California.

Path	Row	Year	Day/month (sensor)	No. scenes
40	36	2002	07/10(ETM+), 12/06(TM)	2
		2003	28/06(TM), 14/07(TM), 15/08(TM), 31/08(TM), 16/09(TM), 02/10(TM), 18/10(TM), 03/11(TM), 19/11(TM), 05/12(TM)	10
40	37	2002	07/10(ETM+), 16/11(TM)	2
		2003	28/06(TM), 14/07(TM), 30/07(TM), 31/08(TM), 16/09(TM), 02/10(TM), 18/10(TM), 19/11(TM), 05/12(TM)	9
41	36	2002	06/10(TM), 15/11(ETM+),	2
		2003	03/06(TM), 19/06(TM), 05/07(TM), 21/07(TM), 06/08(TM), 22/08(TM), 23/09(TM), 09/10(TM), 10/11(TM), 26/11(TM)	10

1995; Martín, 1998; Martín et al., 2005; Pereira, 1999; Smith et al., 2007). The following indices were considered:

(a) VIS + NIR domain: NDVI (Rouse et al., 1974), GEMI (Pinty & Verstraete, 1992) and BAI (Martín, 1998), defined as:

$$NDVI = \frac{\rho_{NIR} - \rho_R}{\rho_{NIR} + \rho_R} \quad (1)$$

$$GEMI = \frac{\eta(1-0.25\eta) - (\rho_R - 0.125)}{(1-\rho_R)} \quad \eta = \frac{2\left(\rho_{NIR}^2 - \rho_R^2\right) + 1.5\rho_{NIR} + 0.5\rho_R}{(\rho_R + \rho_{NIR} + 0.5)} \quad (2)$$

$$BAI = \frac{1}{(\rho_{NIR} - \rho_{cNIR})^2 + (\rho_R - \rho_{cR})^2} \quad (3)$$

where ρ_{NIR} is the reflectance in the NIR, ρ_R is the reflectance in the RED and ρ_{cNIR} and ρ_{cR} are the convergence values (0.06 and 0.1, respectively)

(b) VIS + NIR + 1SWIR. In addition to the input bands of group (a), the Normalized Burn Ratio (NBR) (Key & Benson, 1999) and the improved BAI (BAIM) (Martín et al., 2005) were computed as follows:

$$NBR_S = \frac{\rho_{NIR} - \rho_{SSWIR}}{\rho_{NIR} + \rho_{SSWIR}} \quad (4)$$

$$BAIM_S = \frac{1}{(\rho_{NIR} - \rho_{cNIR})^2 + (\rho_{SSWIR} - \rho_{cSSWIR})^2} \quad (5)$$

where ρ_{NIR} is the reflectance in the NIR, ρ_{SSWIR} is the reflectance in the short SWIR (Landsat TM/ETM+ band 5) and ρ_{cNIR} and ρ_{cSSWIR} are the convergence values (0.05 and 0.2, respectively)

(c) VIS + NIR + 2SWIR. In addition to the input bands of groups (a) and (b) three new indices were added, the long SWIR variation of the NBR and BAIM, using band 7 instead of band 5 of TM/ETM+ (Martín et al., 2005) and the MIRBI (Trigg & Flasse, 2001):

$$NBR_L = \frac{\rho_{NIR} - \rho_{LSWIR}}{\rho_{NIR} + \rho_{LSWIR}} \quad (6)$$

$$BAIM_L = \frac{1}{(\rho_{NIR} - \rho_{cNIR})^2 + (\rho_{LSWIR} - \rho_{cLSWIR})^2} \quad (7)$$

$$MIRBI = 10\rho_{LSWIR} - 9.8\rho_{SSWIR} + 2 \quad (8)$$

where ρ_{NIR} is the reflectance in the NIR, ρ_{LSWIR} is the reflectance in the long SWIR (Landsat TM/ETM+ band 7), ρ_{SSWIR} is the reflectance in the short SWIR and ρ_{cNIR} and ρ_{cLSWIR} are the convergence values (0.05 and 0.2, respectively)

All the aforementioned input variables were computed from both the post-fire image and the multitemporal changes between the post and pre-fire image.

2.5. Phase 1: determination of "core burned" pixels

The determination of seed pixels for burned land mapping was based on an iterative criterion decision method, using a large database of burned and unburned samples extracted from the reference images. About 70,000 burned pixels showing strong magenta colour in TM7-TM4-TM1 RGB post-fire colour composite (Koutsias & Karteris, 2000b) were extracted from the reference images (six small study sites), trying to avoid those located near the patch boundaries, to ensure that only clearly burned pixels were selected. The unburned pixels were selected by a random sampling over the non affected area using the same reference images. The sample size was about twenty times larger than the burned one. The larger database of unburned areas emulates a real situation where this category is more probable and heterogeneous than the burned class. The unburned samples included cloud and cloud-shadows, as well as other land covers that have been reported to produce potential confusions with burned areas: borders of lakes, topographic and cloud shadows and mixed urban-vegetated areas (Chuvieco & Congalton, 1988).

Since this work aimed to classify burned pixels with the lowest possible confusion error, a rule-concatenation methodology was developed to obtain the ideal decision combination that may fulfill that objective. First, the thresholds that allowed selecting a certain burned sample percentage for each variable were extracted (iteratively from 100% to 75%). For each particular percentage, the combination of rules that showed the larger decrement of commission error (percentage of false burned samples) was selected, with a maximum concatenation of four rules to avoid overfitting the dataset. Finally, a cut-off percentage was selected by analyzing the omission and commission errors: whenever a smaller percentage was considered, the thresholds were more severe and the commission error was reduced while the misdetection of burned patches increased. This task was repeated independently with the variables considered in each spectral scenario.

As some decision rules were multitemporal, the seed pixels were obtained applying the criteria over all the combinations between the post-fire scenes (2003) and the previous season scenes (2002), joining the results in a unique raster layer. Performance of this phase was based on three criteria: (a) proportion of burned patches detected (for three different sizes: under 25 ha, from 25–100 ha and above 100 ha); (b) commission error (pixels identified as burned area that were in fact unburned), (c) commission errors by land cover (same as before but classified according to different categories: water, urban areas/bare soils, trees, shrubs, croplands); (d) omission error (true burned pixels not identified as such). This later error was not especially critical in this phase, since the main goal was to reduce false detections.

2.6. Phase 2: shaping the burned areas

The second phase of the burned land mapping algorithm aimed to reduce the omission errors. This phase analyzed the spectral properties of those pixels close to the seed pixels, applying a region-growing algorithm to enlarge the burned patches previously detected. To carry out this phase, we had to select a suitable algorithm, within those proposed for contextual analysis, as well as a suitable band for running that algorithm.

Several contextual algorithms were examined for the region growing process. In image processing literature, spatial segmentation algorithms have been mainly based on three approaches: a) seeded region growing techniques (Adams & Bischof, 1994), based on iterative addition of pixels bordering the seed pixels and with similar spectral characteristics; b) segmentation techniques, which create patches by identifying borders between categories, and c) hybrid techniques that mix both approaches (Baraldi & Parmiggiani, 1996; Pavlidis & Liow, 1990; Rydberg & Borgefors, 2001; Zhang et al., 2005).

After reviewing the advantages and drawbacks of each approach, two fixed region growing algorithms were tested, both with a connectivity of 8 pixels (all pixels in the 3×3 neighbourhood to each seed are considered candidates). In the *Fixed* algorithm, those neighbour pixels were considered burned when they exceed a 35% threshold of probability derived from the logistic regression model and a reflectance in the NIR below 0.25. A hybrid technique was also evaluated, named *Fixed + Borders* algorithm, using an edge detection that combined a low pass Gauss and Sobel edge filters. This process removes the candidate pixels if there is any border in the neighbourhood and includes them with the same fixed probability thresholds

aforementioned. The adaptive threshold methods, where the similarity measures change as new pixels are added to the seeds, were not considered due to their high computational cost.

For optimum algorithm performance, the variable to run the growing process should be sensitive enough to show a clear discrimination between burned and unburned areas, while having simultaneously a low variance within burned areas. Some alternatives were the spectral mixture analysis (Pereira et al., 1999a; Vafeidis & Drake, 2005), classification trees (Maggi & Stroppiana, 2002), logistic regression models (Fraser et al., 2003) or spectral indices based thresholds, for instance the BAI (Garcia & Chuvieco, 2004), GEMI (Chuvieco, Englefield, et al., 2008) or BAIM (Chuvieco, Opazo, et al., 2008).

After testing several of those procedures, we selected a logistic regression approach, which had a long tradition in burned land mapping (Fraser et al., 2003; Koutsias & Karteris, 1998, 2000a; Pu & Gong, 2004; Silva et al., 2004). Input data for the model calibration were the reflective bands and the spectral indices used in the first phase. In this analysis a similar number of burned and unburned samples were used, approximately 60,000, extracted from the set of reference images. The logistic model was computed using a stepwise forward process with a 0.05 significance level and 60% of the samples. The model was tested with the remaining 40%.

The performance of the logistic model was compared with other variables previously used in burned area mapping, such as the post-fire and temporal difference values of the NIR, GEMI, NBR_S, $BAIM_L$, $BAIM_L$ and MIRBI. Model performance was measured using the *Jeffries-Matusita* (JM) distance, defined as:

$$JM = 2\left(1-e^{-B_{ij}}\right) \tag{9}$$

where B_{ij} is the Battacharyya distance, defined as:

$$B_{ij} = \frac{1}{8}\left(m_i-m_j\right)^T\left(\frac{\sum_i+\sum_j}{2}\right)\left(m_i-m_j\right) + \frac{1}{2}\,ln\left[\frac{\left|\left(\sum_i+\sum_j\right)/2\right|}{\left|\sum_i\right|^{1/2}\left|\sum_j\right|^{1/2}}\right] \tag{10}$$

Where m_i and m_j are the vector means of classes i and j, respectively and $\sum_i$ and $\sum_j$ are the covariance matrices of the same classes. JM varies from 0 to 2, and values above 1.9 are generally considered clearly separable (Richards, 1993).

2.7. Aggregation and validation

The results of the algorithms proposed for each scene were summed up, obtaining a unique burned area map for each study site. The raster dataset was then vectorized and aggregated, so all the polygons within the neighbourhood of 100 m were combined into new polygons. The final perimeters were an aggregation of the each those detected in each date, keeping as such the unburned islands. This dataset was compared to the reference cartography for validation, computing error matrices and standard accuracy indices (omission and commission errors and kappa index). The difference in the total area detected for the algorithms in comparison of the official cartography was computed as well.

3. Results

3.1. Results for the first phase

The decision rules with the three spectral groups previously mentioned resulted on the following classification rules:

a) VIS + NIR: Diff_BAI > 144.3835 AND Diff_NDVI < −0.17767 AND Post_NDVI < 0.14413 AND Diff_GEMI < −0.11578
b) VIS + NIR + 1SWIR: $Diff\_BAIM_S > 46.8143$ AND Diff_NDVI < −0.17767 AND $Post\_NBR_S < -0.17079$ AND Post_BAI > 188.88
c) VIS + NIR + 2SWIR: $Diff\_BAIM_L > 56.2384$ AND Diff_NDVI < −0.17767 AND Post_MIRBI > 1.8514 AND $Post\_NBR_L < -0.15006$

Table 4 shows the summary of the results for this first phase. For the reference dataset, the omission and commission errors were generally lower than for the large validation regions (Portugal and Southern California) in all spectral groups. It was evident a decrease in commission errors (which was the target of this phase) by including SWIR bands in the discrimination space (from 26.2 of VIS + NIR to 1.6 of VIS-NIR-1SWIR). For Portugal and Southern California, both the omission and commission errors were higher than for the reference dataset, but significant improvements were also observed when using SWIR bands, specially in the commission errors. In this case, a clear improvement was shown when using two SWIR bands versus just one.

When analyzing results by burned patch size, in Portugal the spectral group 1 reached 99.6% detection rate for fires greater than 100 ha and 95.5% for those between 25 and 100 ha. The detection rate decreased for smaller fires (84.3%). In Southern California the detection rate was 82.1% for patches larger than 100 ha, but decreased notably for smaller fires (34.8% for those between 25 and 100 and 19.0% for those below 25 ha). Commission errors showed to be high in this spectral group, above 40% considering both study areas. These errors were generally associated to confusion with clouds and cloud- or topographic-shadows, as well as with borders of lakes, rivers or coastal areas. Confusion with croplands arose as well in those regions with higher agricultural cover. Omission errors were not very relevant in this phase and, as expected, they were high: 41.5% for Portugal and 83.2% for South-California.

The results of the second spectral group resulted on a similar detection capacity as the first group in Portugal, but were better for South-California with a 5% increase for detecting fires larger than 25 ha, and 10% for those smaller than 25 ha. The commission error of this spectral group improved over the first one, with considerable reductions in the two study sites (Table 4). This should be related mainly to the inclusion of the $Diff\_BAIM_S$ index, which reduces false assignments of clouds and cloud-shadows, as well as with topographic shadows and water, although some confusion was still observed in coastal areas and mixed land–water pixels. Omission errors increased in Portugal and decreased in Southern California, with values higher than 59.6% considering both study areas (Table 4).

The results for the third spectral group clearly improved the performance of the two previous models. The detection of burned patches was similar to the other spectral groups in Southern California, but they were lower in Portugal especially for those below 25 ha, resulting on a decrement of 15%. However, the

Table 4
Omission and commission errors of the first phase for the different spectral spaces.

Study sites	VIS + NIR		VIS + NIR + 1SWIR		VIS + NIR + 2SWIR	
	Omission error (%)	Commission error (%)	Omission error (%)	Commission error (%)	Omission error (%)	Commission error (%)
Reference sample dataset	27.8	26.2	36.8	1.6	33.6	0.2
Portugal	41.5	51.2	59.6	19.8	66.5	3.6
Southern California	83.2	44.8	77.8	10.7	77.0	4.1

commission errors decreased significantly, resulting on values below 5% in both study sites (Table 4). Half of this error was related to croplands, and another important part was located over scrubs, probably due to real fires not included in the validation dataset and geometric misregistration problems between the reference cartography and the Landsat images. There is no evidence of any systematic confusion with other land covers.

3.2. Results for the second phase

Table 5 shows the results of the logistic regression model computed to obtain the variable for the contextual analysis. The selected variables were mostly post-fire indices and input bands (MIRBI, NBR_L, BLUE, $SWIR_S$), but the pre-fire NDVI and NBR_L were selected as well. According to the −2LL change the most significant variables in the model were the post-fire MIRBI, NBR_L and BLUE reflectance. The first two variables represents the two more important spectral regions to detect burned areas from Landsat TM/ETM data, which are the $SWIR_L/SWIR_S$ and $NIR/SWIR_L$, while the Blue channel reduced the confusion with urban/artificial areas and bare soils. The model correctly predicted more than 95% of both burned and unburned sampling pixels, with very low omission (<5%) and commission (<3%) errors. Table 6 shows the results of separability measures after comparing the performance of this model with respect to other variables of potential interest for region growing of the seed pixels; the analysis was based on 25,000 samples extracted using a spatial systematic sampling over the reference sites. Fig. 2 shows a representative example of a large fire in San Diego County (California). As it is shown, the logistic model obtains the higher JM scores not only in the reference images, but also in both validation sites, with values higher than 1.93.

The two region growing algorithm (*Fixed* and *Fixed + borders*) showed significant improvements over the first phase in terms of omission errors and global accuracy (Table 7). The increase in the Kappa index was significant in both cases ($p<0.05$). Omission errors were reduced by more than 50% in both study sites. In the negative side, commission errors increased as well but in a fairly low proportion and depending on the algorithm considered: the *Fixed + Borders* algorithm showed lower commission errors (<16.5%) in comparison with the *Fixed* algorithm (<32.2%) (see Fig. 3), which also implies a better general agreement (Kappa = 0.85 for *Fixed + Borders*, while Kappa >0.77 for *Fixed*). Comparing with reference cartography, *Fixed + Borders* overestimated 27,574 ha in Portugal and underestimated 13,077 ha in Southern California, while *Fixed* overestimated more than 165,000 and 31,000 ha respectively (Table 7). In addition, *Fixed + Borders* was computationally more efficient when less candidate pixels were evaluated. The Fig. 4 shows a general view of the burned cartography obtained by *Fixed + Borders* algorithm in the validation sites.

Considering both study areas, the confusion in croplands showed to be responsible for more than 50% of the resulting commission error. Removing the areas detected for the algorithm mainly in agricultural areas (using land cover cartography and considering a minimum membership of 90%), the commission error improved significantly ($p<0.05$) obtaining kappa values >0.87, maintaining similar omission errors.

Table 5
Logistic regression model.

Variables	B	S.E.	Wald	Sig.	Change in the −2LL when removing the variable
MIRBI_post	11.805	0.130	8241.4	0.00	12,715.9
NBRL_post	−11.845	0.146	6575.8	0.00	10,424.3
BLUE_post	−102.827	1.717	3587.4	0.00	5967.5
SWIRs_post	20.377	0.476	1833.7	0.00	2105.4
NBRL_pre	5.844	0.147	1574.1	0.00	1684.0
NDVI_pre	5.001	0.180	771.4	0.00	876.7
Constant	−15.500	0.245	4012.2	0.00	

4. Discussion

This paper has presented a two phase methodology to confidently map burned areas from Landsat TM-ETM+ images. The methods have been develop for six reference Landsat scenes in the Mediterranean basin and applied to two regional study sites to check consistency and generalizing power.

Many authors have recognized that burned patches do not present a specific spatial pattern (Smith et al., 2002) and therefore the discrimination of those areas should be based on either spectral or temporal contrast (or rather in both). Considering the wide variety of spectral characteristics within a burned patch (char, scorched leaves or grass, or even green leaves when the fire is not very severe), the detection of burned areas is not a trivial task. When applying very strict algorithms, false alarms are reduced at the expense of reducing the detection of true-burned areas. The opposite occurs when applying less severe algorithms, which are commonly complemented by different filters that try to remove potential confusions (water or cropland masks, for instance).

The two-phase approach presented in this paper reduces both problems associated to over and underestimation. The first phase tries to identify the most clearly burned pixels within each burned patch, while the second one improves the discrimination by analyzing the spectral properties of only the pixels nearby those identified in the first phase. Since conceptually speaking the aim is different in both phases, the methods and input bands to obtain those goals should also be different. The first phase requires a technique that emphasizes the internal differences within the burned area (to extract the most clearly burned), while the latter reduces those differences and increase them with the unburned surrounding environment.

Following this logic, two different techniques have been applied in this case. In the first phase, a decision rule combination method has been developed to try to establish the concatenation of rules that minimize the confusion with not burned areas. An alternative process would be to apply classification trees (Breiman et al., 1984), but this technique is oriented to balance omission and commission errors and it wasn't appropriate to reach our goal. Thresholds for the different spectral variables considered had been extracted so that they selected the 85% of reference burned samples. That value was considered adequate as the best commission errors obtained in the reference samples were considered operative and below 0.1%.

Among the three spectral spaces tested, the best results were obtained with VIS + NIR + 2SWIR, which reduced the confusions with water, shadows and agricultural areas observed in the other spectral spaces. This implies that MODIS and Landsat TM-ETM+ are currently the only sensors that provide the ideal spectral resolution for the accurate discrimination of burned areas. Other sensors with only one band in the SWIR should present a lower ability to detect burned areas maintaining low commission errors. This is the case of VEGETATION or HRVIR, the AWIFS, AATSR and AVHRR. Other sensors which do not even have the SWIR (such as the DMC constellation) should present a lower performance, although it should be checked whether the improvement in temporal resolution may compensate this deficiency.

The spectral indices that more clearly contribute to the discrimination of burned pixels were the multitemporal difference of BAI and BAIM (either computed with SWIR bands 5 and 7), which were selected in the first stage of decision rule combination in the three spectral groups. Later, NDVI difference was also included in the three groups, reducing the confusion with urban areas and other not combustible land covers. Additional variables were introduced in later stages to amend some of the potential confusions with other land covers. In the VIS + NIR group, the Post NDVI and GEMI difference

Table 6
Separability values (JM distances) between burned and unburned pixels in different unitemporal (Post-fire) and multitemporal (Diff = Post–Pre Fire) variables.

	Logistic model	NIR		NDVI		NBR_S		NBR_L		$BAIM_L$		MIRBI	
		Post	Diff	Post	Diff	Post	Diff	Post	Diff	Post	Diff	Post	Diff
Reference sample dataset	2	1.06	0.44	0.82	0.91	1.20	1.17	1.53	1.51	1.35	1.39	1.41	1.40
Portugal	1.93	0.50	0.21	0.86	0.46	1.18	0.43	1.33	0.61	1.21	1.13	0.50	0.69
Southern California	1.95	0.44	0.16	0.48	0.30	1.09	0.35	1.05	0.48	1.37	1.30	0.60	0.44
Average	1.96	0.67	0.27	0.72	0.56	1.16	0.65	1.30	0.87	1.31	1.27	0.84	0.84

reduced slightly the problems with dark surfaces (shadows and water). In the VIS + NIR + 1SWIR the post NBR_S, BAI and MIRBI and NBR_L variables in the VIS + NIR + 2SWIR group were selected for the same purpose, trying to overcome the confusion with urban and cropland areas. The MIRBI index was shown to be a critic variable with an excellent ability to reduce the confusions with mixed pixels found in water–land borders, areas affected in previous fire seasons and arable land areas. In contrast, it caused a decrement in the detection rate, especially for the smaller fires. This behaviour was observed clearly in Portugal, with a 15% reduction of detection rate for fires <25 ha.

The second phase of the proposed methodology was found to be critical for reducing the omission errors, but the choice of the region-growing algorithm was less important than the actual detection of seed pixels of the first phase and the absence of commission errors. The contextual algorithms were found very dependent on the spatial configuration of the seed pixels. The algorithms tested in this paper significantly reduced the omission errors, while increasing slightly the commission errors over the first phase. For running those algorithms the user first needs to define an input variable to start the growing process. The ideal candidate for this task is a variable that shows a strong separability between burned and unburned pixels, while keeping a low variance within the burned area. The burned probability produced by our logistic probability image produced higher separability than other variables, while facilitating the establishment of adequate cut-off values for different burning conditions.

The two region growing algorithms evaluated were based on a fixed cut-off value of 35% of output probability, a quite low value oriented to reduce the omission error. The NIR<0.25 criterions allowed to reduce the confusion mainly with arable lands. The *Fixed* region growing algorithm showed more dependence than the *Fixed + Borders* algorithm to the probability threshold: the Sobel edge detector (before homogenised with a Gaussian filter to extract cleaner borders) allowed to detect the pixels with a local variability by identifying abrupt changes in its local vicinity within a mobile window of 3 × 3, allowing a more accurate stop of the region growing process. Object classification strategies rely on a similar assumption, considering as many seeds as pixels at the beginning of the process, locating the local edges in a natural way (Mitri & Gitas, 2004;

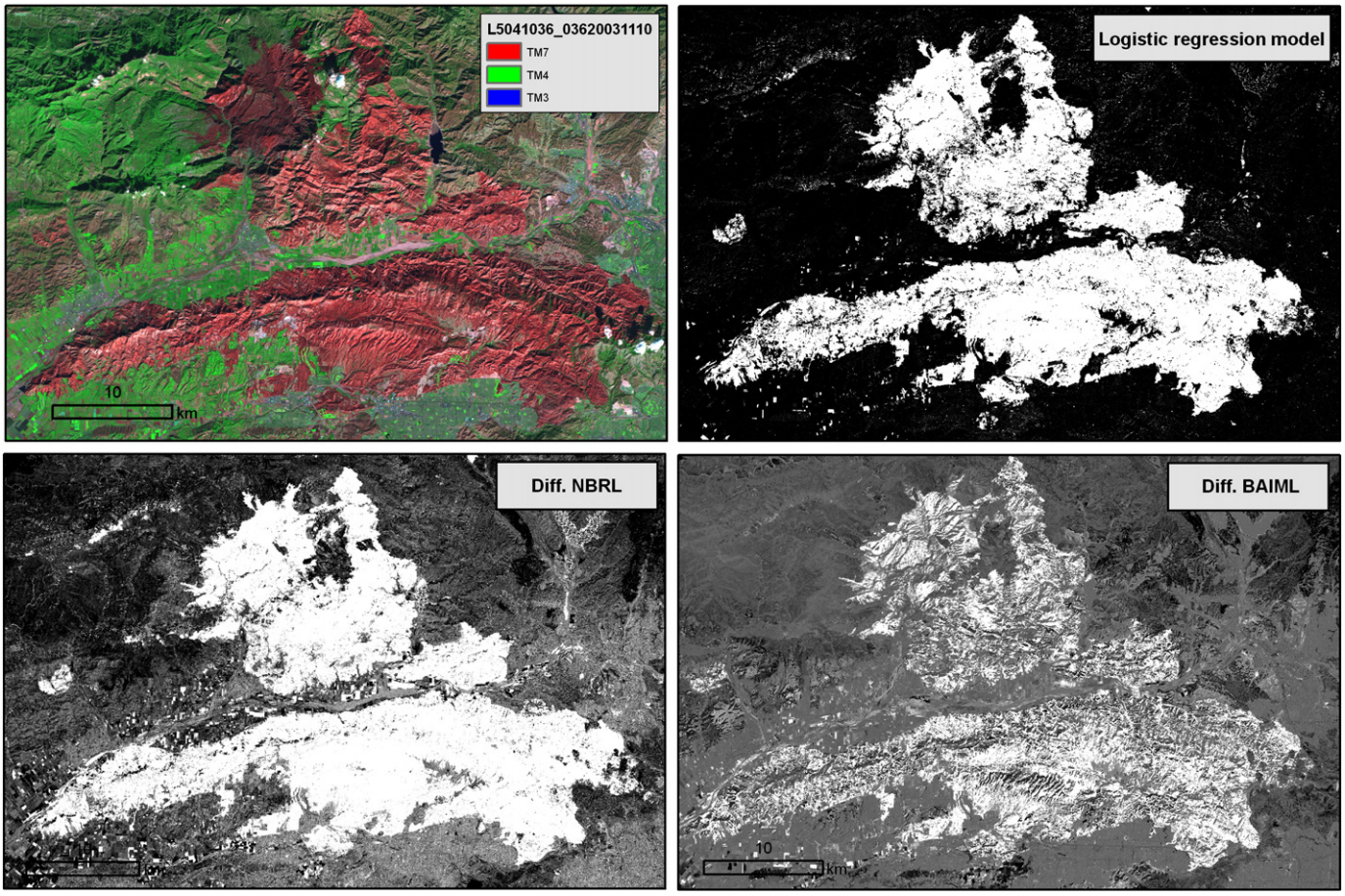

Fig. 2. Comparison between logistic regression model predicted probability, NBR_L and $BAIM_L$ multitemporal difference over Cedar Fire (San Diego County–California).

Table 7
Omission (OE) and Commission (CE) errors, kappa values and the difference with the reference area (Dif) for the first phase and the region growing algorithms for the different study sites.

Study area	Seeds (first phase)				Fixed algorithm				Fixed + borders algorithm			
	OE (%)	CE (%)	Kappa	Dif (ha)	OE (%)	CE (%)	Kappa	Dif (ha)	OE (%)	CE (%)	Kappa	Dif (ha)
Portugal	66.5	3.6	0.48	−287,177	6.3	32.2	0.77	165,787	11.1	16.5	0.85	27,574
Southern California	77.0	4.1	0.36	−238,067	11.4	19.6	0.84	31,256	15.7	12.1	0.85	−13,077

Quintano et al., 2006) but this approach is computational less efficient for an operational application.

The commission errors observed by using the *Fixed + Borders* algorithm in both study areas was mostly related with croplands, especially with arable lands, as they showed very similar spectral and temporal behaviour to burned areas, especially for dark soils. The abrupt change between crops limits helped to restrict the growing process. Even with *Fixed + Borders* algorithm more than half of the commission error was found in this land cover, mainly as consequence of erroneously located seeds in the first phase. The other half of the commission errors was located over scrub and forested areas, and they were partially related to the unburned patches within the reference perimeters. In fact, the Southern California perimeters do not include any "islands" within burned patches, and only the bigger ones are considered in Portugal, causing the increase of the omission errors as well. The misregistration of the data sources compared, the missed or incomplete fires and the detection of old burned areas may also be responsible for these errors.

The kappa values for the results of the second phase showed high agreement with the borders approach (0.85, for both study areas), with an overestimation of almost 30,000 ha in Portugal and an underestimation of less than the half in Southern California. However, it was observed that the region growing algorithms performed much better when the burned patch was compact and had few internal islands, so there was good spatial connectivity between the seeds and the burned area. This option was more critical when the edge of the burned patch had similar spectral characteristics, since the filter helped to restrict the growing to the actual limits of the fire.

Both phases of the described algorithm, particularly the first one are dependent of the acquisition time after the fire: wherever the ecosystem succession after fire is quick, the signal is weakened, especially for smaller ones that are not usually detected. To overcome this dependence, the proposed methodology works with the maximum number of available scenes, making more probable to find a stronger burned signal in short-term post fire conditions. This strategy avoids as well the need to make a manual selection of post-fire scenes, thus facilitating a fully automatic process.

The global accuracy of the two-phase method proposed in this paper was high and consistent throughout two regional study sites that cover large regions 70,000 km^2 in South-California and

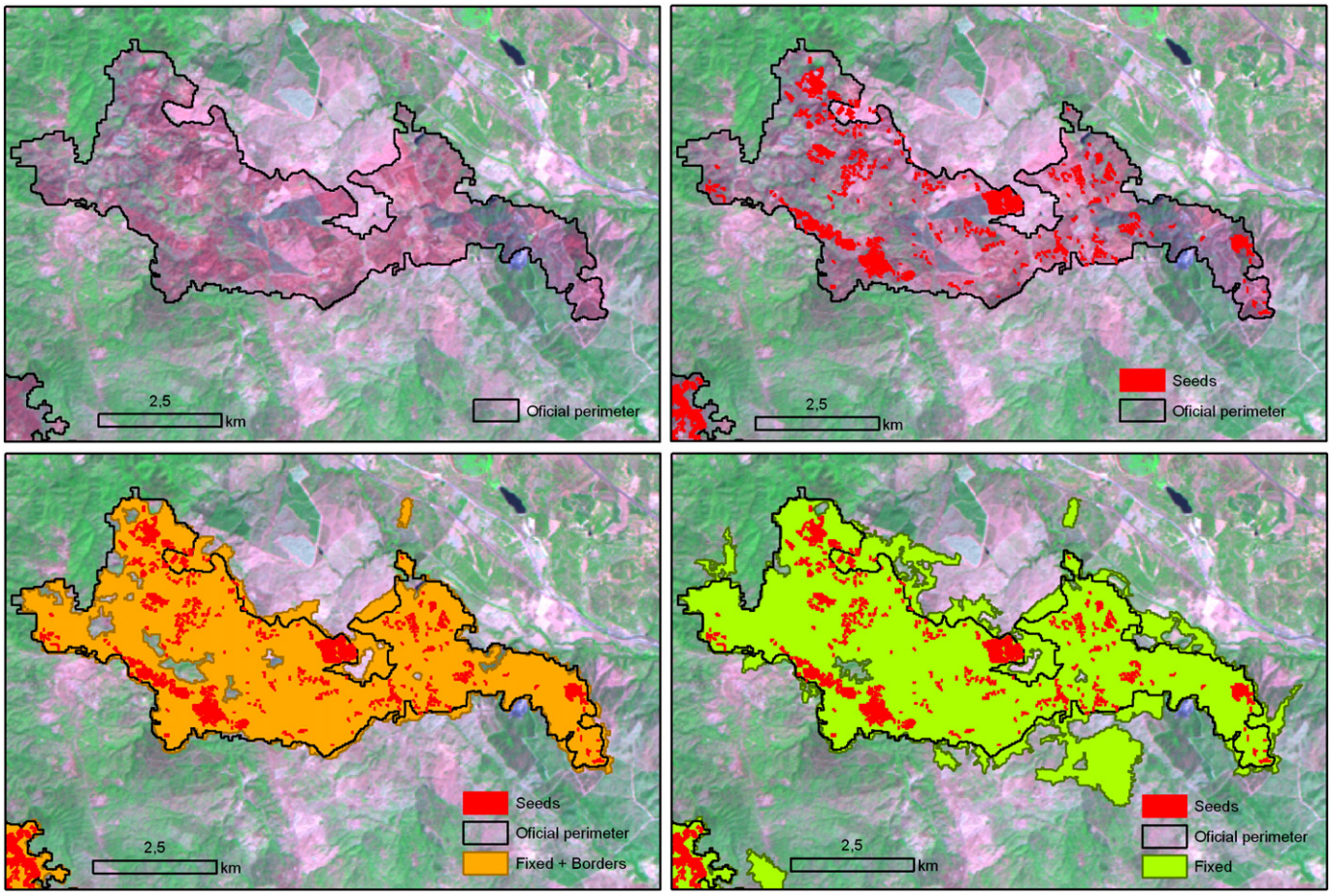

Fig. 3. Seeds and results from the region growing algorithms for a burned area in Portugal. Examples from *Fixed* and *Fixed + Borders* algorithms are shown.

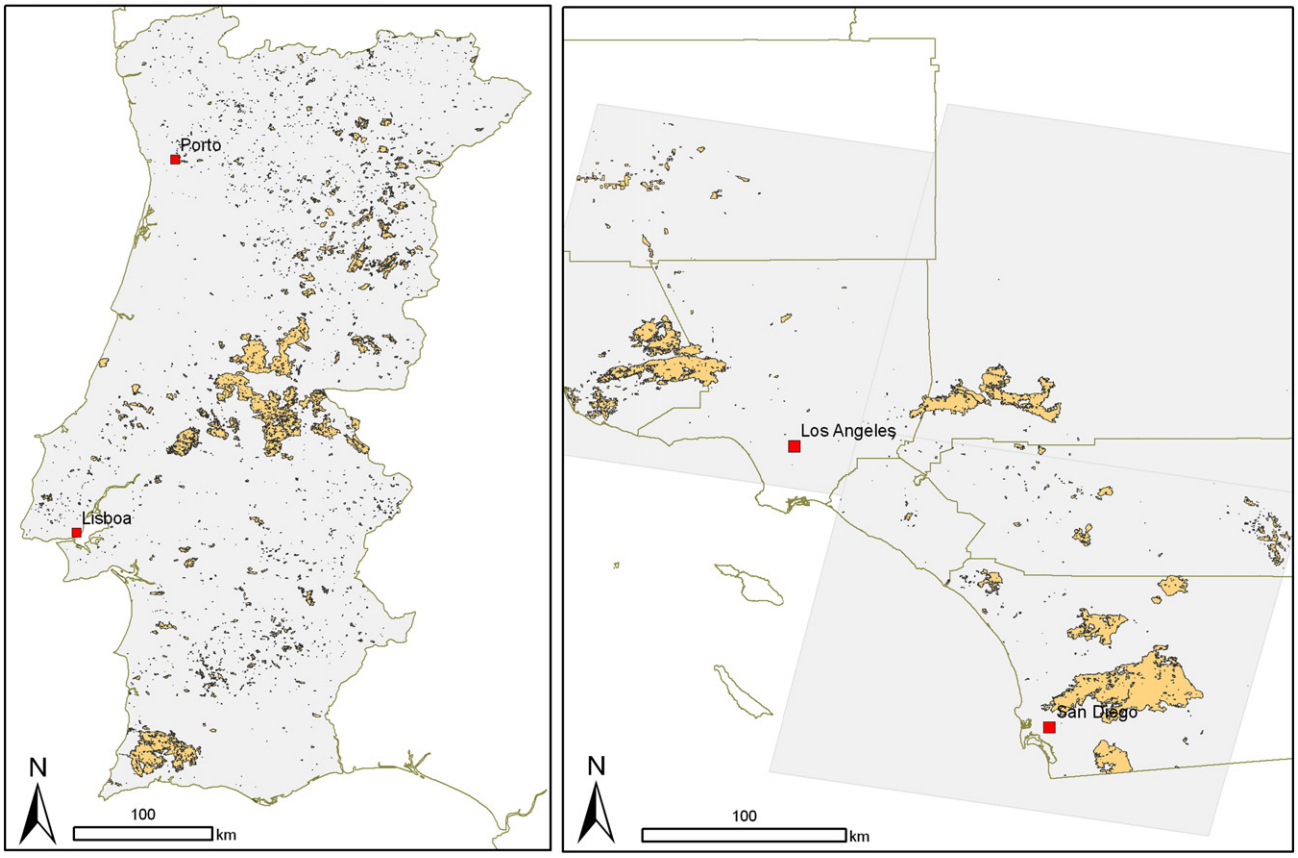

Fig. 4. *Fixed + Borders* algorithm final result in the two study areas.

89,000 km^2 in Portugal, and should be a good alternative to automate the burned scar mapping process at a country scale. The comparison of our results with those obtained from previously published studies showed similar or slightly higher accuracy (Kappa >0.9) but, as mentioned previously, most of the published studies with Landsat images are based in local fires, and therefore the generalization capacity of the proposed algorithms was not really tested.

Both tested regions (Portugal and California) have a Mediterranean climate, and have similarities in terms of vegetation and fire regime conditions. Additional studies should be performed on whether the same methods can be confidently applied to tropical or boreal ecosystems.

5. Conclusions

This paper has shown the results of applying a two-phase methodology to mapping burned areas with medium resolution satellite images (Landsat TM/ETM+). The first phase was aimed to detect the most clearly burned pixels (core burned), and it was based on spectral–temporal rule combination analysis. The second phase was based on the application of region-growing algorithms, which makes it possible to incorporate the spatial properties for discrimination of burned patches.

The accuracies of both phases were found very high and consistent throughout two regional study sites. The first phase had very low commission errors, while the second one reduced significantly the omission errors, obtaining a final kappa higher than 0.85. The developed methodology showed to be more accurate for compact shaped burned areas outside cropland where the spectral behaviour is similar.

In summary, the two-phase algorithm approach presented in this paper provided an accurate automatic mapping of burned areas. This method can be operationally used at temperate ecosystems, although we plan to further test it for other ecosystems as well. Future work is focused to reduce the commission errors observed at croplands.

References

Adams, R., & Bischof, L. (1994). Seeded region growing. *IEEE Transactions on Pattern Analysis and Machine Intelligence*, *16*, 641−647.

Baraldi, A., & Parmiggiani, F. (1996). Single linkage region growing algorithms based on the vector degree of match. *IEEE Transactions on Geoscience and Remote Sensing*, *34*, 137−148.

Barbosa, P. M., Gregoire, J. -M., & Pereira, J. M. C. (1999). An algorithm for extracting burned areas from time series of AVHRR GAC data applied at a continental scale – An overview. *Remote Sensing of Environment*, *69*, 253−263.

Breiman, L., Friedman, J. H., Olshen, R. A., & Stone, C. J. (1984). *Classification and regression trees.* Belmont, CA: Wadsworth.

Chander, G., Markham, B. L., & Helder, D. L. (2009). Summary of current radiometric calibration coefficients for Landsat MSS, TM, ETM+, and EO-1 ALI sensors. *Remote Sensing of Environment*, *113*(113), 893−903.

Chuvieco, E. (2008). Satellite observation of biomass burning: implications in global change research. In E. Chuvieco (Ed.), *Earth Observation and Global Change* (pp. 109−142). New York: Springer.

Chuvieco, E., & Congalton, R. G. (1988). Mapping and inventory of forest fires from digital processing of TM data. *Geocarto International*, *4*, 41−53.

Chuvieco, E., Martín, M. P., & Palacios, A. (2002). Assessment of different spectral indices in the red-near-infrared spectral domain for burned land discriminations. *International Journal of Remote Sensing*, *23*, 5103−5110.

Chuvieco, E., Riaño, D., Danson, F. M., & Martín, M. P. (2006). Use of a radiative transfer model to simulate the post-fire spectral response to burn severity. *Journal of Geophysical Research - Biosciences*, *111*. doi:10.1029/2005JG000143

Chuvieco, E., Englefield, P., Trishchenko, A. P., & Luo, Y. (2008). Generation of long time series of burn area maps of the boreal forest from NOAA–AVHRR composite data. *Remote Sensing of Environment*, *112*, 2381−2396.

Chuvieco, E., Opazo, S., Sione, W., Del Valle, H., Anaya, J., Di Bella, C., et al. (2008). Global Burned Land Estimation in Latin America using MODIS Composite Data. *Ecological Applications*, *18*, 64−79.

Fernández, A., Illera, P., & Casanova, J. L. (1997). Automatic mapping of surfaces affected by forest fires in Spain using AVHRR NDVI composite image data. *Remote Sensing of Environment*, *60*, 153−162.

Fraser, R. H., Fernandes, R., & Latifovic, R. (2003). Multi-temporal mapping of burned forest over Canada using satellite-based change metrics. *Geocarto International*, *18*, 37−47.

Garcia, M., & Chuvieco, E. (2004). Assessment of the potential of SAC-C/MMRS imagery for mapping burned areas in Spain. *Remote Sensing of Environment*, *92*, 414−423.
Global Climate Observing System (GCOS) (2006). Systematic Observation Requirements for Satellite-based products for Climate – Supplemental Details to the GCOS Implementation Plan. World Meteorological Organization.
Homer, C., Dewitz, J., Fry, J., Coan, M., Hossain, N., Larson, C., et al. (2007). Completion of the 2001 National Land Cover Database for the Conterminous United States. *Photogrammetric Engineering and Remote Sensing*, *73*, 337−341.
Hudak, A. T., & Brockett, B. H. (2004). Mapping fire scars in a southern African savannah using Landsat imagery. *International Journal of Remote Sensing*, *25*, 3231−3243.
Kasischke, E. S., & French, N. H. F. (1995). Locating and estimating the areal extent of wildfires in Alaskan boreal forests using multiple-season AVHRR NDVI composite data. *Remote Sensing of Environment*, *51*, 263−275.
Key, C. H., & Benson, N. C. (1999). *The Normalized Burn Ratio (NBR): A Landsat TM radiometric measure of burn severity*. U.S. Department of the Interior, Northern Rocky Mountain Science Centre.
Koutsias, N., & Karteris, M. (1998). Logistic regression modelling of multitemporal Thematic Mapper data for burned area mapping. *International Journal of Remote Sensing*, *19*, 3499−3514.
Koutsias, N., & Karteris, M. (2000a). Burned area mapping using logistic regression modeling of a single post-fire Landsat-5 Thematic Mapper image. *International Journal of Remote Sensing*, *21*, 673−687.
Koutsias, N., & Karteris, M. (2000b). Burned area mapping using logistic regression modeling of a single post-fire Landsat-5 Thematic Mapper image. *International Journal of Remote Sensing*, *21*, 673−687.
Maggi, M., & Stroppiana, D. (2002). Advantages and drawbacks of NOAA-AVHRR and SPOT-VGT for burnt area mapping in a tropical savanna ecosystem. *Canadian Journal of Remote Sensing*, *28*, 231−245.
Martín, M.P. (1998). Cartografía e inventario de incendios forestales en la Península Ibérica a partir de imágenes NOAA-AVHRR. Ph.D. dissertation Universidad de Alcalá, Alcalá de Henares
Martín, M. P., Gómez, I., & Chuvieco, E. (2005). Performance of a burned-area index (BAIM) for mapping Mediterranean burned scars from MODIS data. In J. Riva, F. Pérez-Cabello, & E. Chuvieco (Eds.), *Proceedings of the 5th International Workshop on Remote Sensing and GIS applications to Forest Fire Management: Fire Effects Assessment* (pp. 193−198). Paris: Universidad de Zaragoza, GOFC-GOLD, EARSeL.
Mitri, G. H., & Gitas, I. Z. (2004). A performance evaluation of a burned area object-based classification model when applied to topographically and non-topographically corrected TM imagery. *International Journal of Remote Sensing*, *25*, 2863−2870.
Palacios-Orueta, A., Chuvieco, E., Parra, A., & Carmona-Moreno, C. (2005). Biomass burning emissions: A review of models using remote-sensing data. *Environmental Monitoring and Assessment. Environmental Monitoring and Assessment*, *104*, 189−209.
Pavlidis, T., & Liow, Y. T. (1990). Integrating region growing and edge detection. *IEEE Transactions on Pattern Analysis and Machine Intelligence*, *12*, 225−233.
Pereira, J. M. C. (1999). A comparative evaluation of NOAA/AVHRR vegetation indexes for burned surface detection and mapping. *IEEE Transactions on Geoscience and Remote Sensing*, *37*, 217−226.
Pereira, M. C., & Setzer, A. W. (1993). Spectral characteristics of fire scars in Landsat-5 TM images of Amazonia. *International Journal of Remote Sensing*, *14*, 2061−2078.
Pereira, J. M. C., Sa, A. C. L., Sousa, A. M. O., Martín, M. P., & Chuvieco, E. (1999). Regional-scale burnt area mapping in Southern Europe using NOAA-AVHRR 1 km data. In E. Chuvieco (Ed.), *Remote Sensing of Large Wildfires in the European Mediterranean Basin* (pp. 139−155). Berlin: Springer-Verlag.
Pereira, J. M. C., Sa, A. C. L., Sousa, A. M. O., Silva, J. M. N., Santos, T. N., & Carreiras, J. M. B. (1999). Spectral characterisation and discrimination of burnt areas. In E. Chuvieco (Ed.), *Remote Sensing of Large Wildfires in the European Mediterranean Basin* (pp. 123−138). Berlin: Springer-Verlag.
Pinty, B., & Verstraete, M. M. (1992). GEMI: a non-linear index to monitor global vegetation from satellites. *Vegetatio*, *101*, 15−20.
Pu, R., & Gong, P. (2004). Determination of burnt scars using logistic regression and neural network techniques from a single post-fire Landsat-7 ETM+ image. *Photogrammetric Engineering and Remote Sensing*, *70*, 841−850.
Quintano, C., Fernández-Manso, A., Fernández-Manso, O., & Shimabukuro, Y. E. (2006). Mapping burned areas in Mediterranean countries using spectral mixture analysis from a uni-temporal perspective. *International Journal of Remote Sensing*, *27*, 645−662.
Randerson, J. T., van der Werf, G. R., Collatz, G. J., Giglio, L., Still, C. J., Kasibhatla, P., et al. (2005). Fire emissions from C3 and C 4 vegetation and their influence on interannual variability of atmospheric CO2 and D13 CO2. *Global Biogeochemical Cycles*(GB2019). doi:10.1029/2004GB002366
Riaño, D., Ruiz, J. A. M., Isidoro, D., Ustin, S. L., & Riaño, D. (2007). Global spatial patterns and temporal trends of burned area between 1981 and 2000 using NOAA-NASA Pathfinder. *Global Change Biology*, *13*, 40−50.
Richards, J. A. (1993). *Remote Sensing Digital Image Analysis. An Introduction.* Berlin: Springer-Verlag.
Rosenqvist, Å., Milne, A., Lucas, R., Imhoff, M., & Dobson, C. (2003). A review of remote sensing technology in support of the Kyoto Protocol. *Environmental Science & Policy*, *6*, 441−445.
Rouse, J. W., Haas, R. W., Schell, J. A., Deering, D. H., & Harlan, J. C. (1974). Monitoring the vernal advancement and retrogradation (Greenwave effect) of natural vegetation. Greenbelt, MD. USA: NASA/GSFC.
Roy, D. P., & Boschetti, L. (2009). Southern Africa validation of the MODIS, L3JRC and GlobCarbon burned-area products. *IEEE Transactions on Geoscience and Remote Sensing*, *47*. doi:10.1109/TGRS.2008.2009000
Roy, D., Jin, Y., Lewis, P. E., & Justice, C. O. (2005). Prototyping a global algorithm for systematic fire-affected area mapping using MODIS time series data. *Remote Sensing of Environment*, *97*, 137−162.
Roy, D. P., Boschetti, L., & Justice, C. O. (2008). The collection 5 MODIS burned area product − Global evaluation by comparison with the MODIS active fire product. *Remote Sensing of Environment*, *112*, 3690−3707.
Russel-Smith, J., Ryan, P. G., & Durieu, R. (1997). A Landsat MSS-derived fire history of Kakadu National Park, monsoonal northern Australia 1980–94: seasonal extent, frequency and patchiness. *Journal of Applied Ecology*, *35*, 829−846.
Russel-Smith, J., Ryan, P. G., & Cheal, D. C. (2002). Fire regimes and the conservation of sandstone heath in monsoonal northern Australia: Frequency, interval, patchiness. *Biological Conservation*, *104*, 91−106.
Rydberg, A., & Borgefors, G. (2001). Integrated method for boundary delineation of agricultural fields in multispectral satellite images. *IEEE Transactions on Geoscience and Remote Sensing*, *39*, 2514−2520.
Silva, J. M. N., Cadima, J. F. C. L., Pereira, J. M. C., & Gregoire, J. M. (2004). Assessing the feasibility of a global model for multi-temporal burned area mapping using SPOT-VEGETATION data. *International Journal of Remote Sensing*, *25*, 4889−4913.
Smith, A. M. S., Wooster, M. J., Powell, A. K., & Usher, D. (2002). Texture based feature extraction: application to burn scar detection in Earth observation satellite sensor imagery. *International Journal of Remote Sensing*, *23*, 1733−1739.
Smith, A. M. S., Drake, N. A., Wooster, M. J., Hudak, A. T., Holden, Z. A., & Gibbons, C. J. (2007). Production of Landsat ETM+ reference imagery of burned areas within Southern African savannahs: comparison of methods and application to MODIS. *International Journal of Remote Sensing*, *28*, 2753−2775.
Tansey, K., Grégoire, J. M., Defourny, P., Leigh, R., Peckel, J. F., Bogaert, E. V., et al. (2008a). A new, global, multi-annual (2000–2007) burnt area product at 1 km resolution. *Geophysical Research Letters*, *35*, L01401. doi:10.1029/2007GL03156
Tansey, K., Grégoire, J. M., Defourny, P., Leigh, R., Peckel, J. F., Bogaert, E. V., et al. (2008b). A new, global, multi-annual (2000–2007) burnt area product at 1 km resolution. *Geophysical Research Letters*, *35*. doi:10.1029/2007GL03156
Thonicke, K., Spessa, A., Prentice, I. C., Harrison, S. P., Dong, L., & Carmona-Moreno, C. (2010). The influence of vegetation, fire spread and fire behaviour on biomass burning and trace gas emissions: Results from a process-based model. *Biogeosciences*, *7*, 697−743.
Trigg, S., & Flasse, S. (2001). An evaluation of different bi-spectral spaces for discriminating burned shrub-savannah. *International Journal of Remote Sensing*, *22*, 2641−2647.
Vafeidis, A. T., & Drake, N. A. (2005). A two-step method for estimating the extent of burnt areas with the use of coarse-resolution data. *International Journal of Remote Sensing*, *26*, 2441−2459.
Zhang, Q., Pavlic, G., Chen, W., Fraser, R. H., Leblanc, S., & Cihlar, J. (2005). A semi-automatic segmentation procedure for feature extraction in remotely sensed imagery. *Computers and Geosciences*, *31*, 289−296.